Check for updates

A tris-spiro metalla-aromatic system featuring Craig-Möbius aromaticity

Zhe Huang [1], Yongliang Zhang[1], Wen-Xiong Zhang [1], Junnian Wei[1✉], Shengfa Ye [2,3✉] & Zhenfeng Xi [1,4✉]

As aromaticity is one of the most fundamental concepts in chemistry, the construction of aromatic systems has long been an important subject. Herein, we report the synthesis and characterization of a tris-spiroaromatic complex, hexalithio spiro vanadacycle **2**. The delocalization of the four electrons within the two V 3d orbitals and the π^* orbitals of the three biphenyl ligands leads to a 40π Craig-Möbius aromatic system with three metalla-aromatic rings, as revealed by both experimental measurements and theoretical analyses. For comparison, if Cr is used instead of V, a similar Craig-Möbius aromatic system can not be generated. In this case, pentalithio spiro chromacycle **3** is obtained, and the Cr center uses its two 3d orbitals to form two independent metalla-aromatic rings. This work presents a type of aromatic systems that will contribute to both aromaticity theory and organometallic chemistry.

[1] Beijing National Laboratory for Molecular Sciences (BNLMS), Key Laboratory of Bioorganic Chemistry and Molecular Engineering of Ministry of Education, College of Chemistry, Peking University, Beijing 100871, China. [2] State Key Laboratory of Catalysis, Dalian Institute of Chemical Physics, Chinese Academy of Sciences, 457 Zhongshan Road, Dalian 116023, China. [3] Max-Planck-Institut für Kohlenforschung, Kaiser-Wilhelm-Platz 1, D-45470, Mülheim an der Ruhr, Germany. [4] State Key Laboratory of Organometallic Chemistry, Shanghai Institute of Organic Chemistry, Chinese Academy of Sciences, Shanghai 200032, China. ✉email: jnwei@pku.edu.cn; shengfa.ye@dicp.ac.cn; zfxi@pku.edu.cn

Aromaticity is one of the most long-standing and funda-mental concepts in chemistry[1–7]. While the original stu-dies mainly focused on conventional organic aromatic compounds, the introduction of transition metals into aromatic systems has brought about fascinating metalla-aromatic struc-tures that are distinct from their corresponding hydrocarbon analogs, mostly because of the participation of *d* orbitals[8–19]. For example, the term spiroaromaticity was first introduced to describe spirocyclic compounds with homoconjugation, in which the spiro *sp*³ carbon atom is not involved[20–22]. In 2002, Rzepa proposed that the spiro atom itself could participate in the con-jugation to form a class of spiroaromatic systems in which each ring could sustain aromaticity independently[23,24] or join together to exhibit global aromaticity[25]. This type of spiroaromaticity could not be achieved when the spiro atom is carbon, which has only four valence orbitals. However, by employing transition metals as the spiro atom, we have realized two types of bis-spiro metalla-aromatics with square planar (Type I, Fig. 1a)[18] and tetrahedral (Type II, Fig. 1a) geometries[19]. The *d* electron con-figurations of the metal centers were found to be a critical factor that largely dictates their geometric and electronic structures. Accordingly, we surmised that to further construct tris-spiro metalla-aromatic structures, the metal center needs to possess more empty *d*-orbitals, which prompted us to turn our attention to early transition metals.

Rzepa et al. have theoretically studied a number of tris-spiroaromatic candidates having P, As, or V as the spiro atom, which exhibit a certain degree of aromaticity[24,25], but none of

them has been realized yet. Although Craig-Möbius type mole-cular orbitals were found in Ta(DAD)₃⁺ (DAD = 1,4-diazabuta-1,3-diene)[25,26], no other proofs have been provided to support its aromaticity. Besides, the presence of Möbius type orbitals in metallacycles is only a necessary condition, rather than a suffi-cient one, for Möbius aromaticity, because Hückel aromatic systems with transition metals may also involve such orbitals, as demonstrated by Mauksch and Tsogoeva[9].

Herein we report hexalithio spiro vanadacycle **2** as a tris-spiro metalla-aromatic compound (Type III, Fig. 1a). The V atom uses its two 3*d* orbitals to interact with the π* orbital of the three biphenyl ligands; consequently, the resulting three metalla-aromatic rings as a whole lead to a 40π Craig-Möbius aromatic system. For comparison, pentalithio spiro chromacycle **3** is also synthesized, in which the Cr atom employs its two 3*d* orbitals to form two independent metalla-aromatic rings.

Results
Synthesis. Although the previous spiro metalla-aromatics were synthesized from 1,4-dilithio-1,3-butadienes in our group[18,19], similar attempts with early transition metals failed, probably due to the presence of redox side-reactions. We then turned to 2,2′-dilithiobiphenyl **1**[27,28], another potential non-innocent ligand with a similar π* orbital, which has been utilized to synthesize aromatic 9-germafluorenyl[29] and 9-stannafluorenyl dianions[30]. As shown in Fig. 1b, the reaction of **1** with 0.33 equivalents of VCl₃(THF)₃ and an excess amount of metallic lithium in the

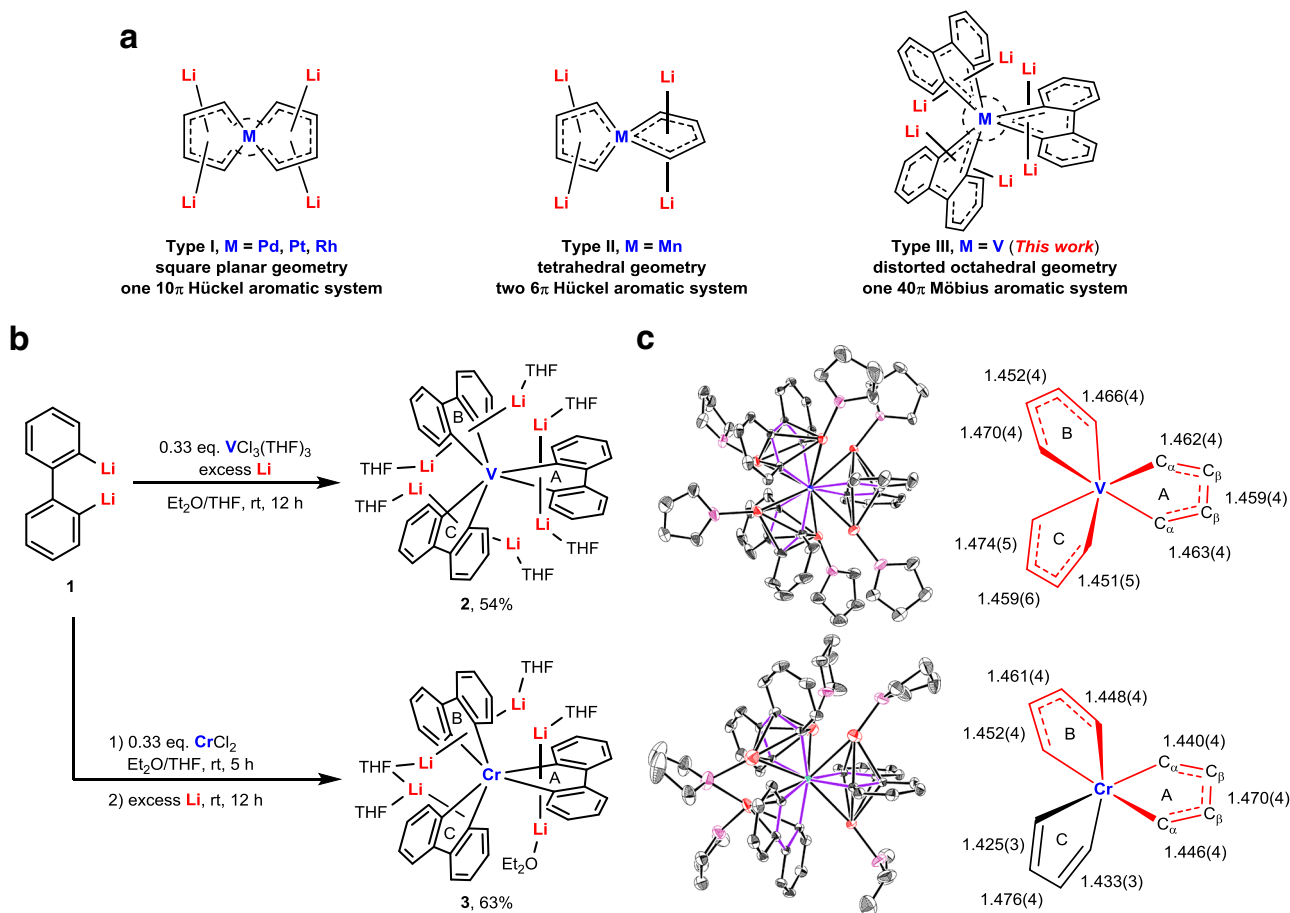**Fig. 1 Synthesis and molecular structures of hexalithio spiro vanadacycle 2 and pentalithio spiro chromacycle 3. a**, Three types of spiro metalla-aromatics. **b**, Synthesis of complexes **2** and **3**. **c**, X-ray molecular structures of complexes **2** and **3** drawn with 30% thermal ellipsoids and selected bond lengths (Å). Hydrogen atoms are omitted for clarity. Metalla-aromatic rings are drawn in red.

mixed solvent of Et_2O and THF (3:1) at room temperature afforded hexalithio spiro vanadacycle **2** in 54% isolated yield as dark blue crystals. Although a similar three-component reaction using $CrCl_2$ instead of $VCl_3(THF)_3$ did not give any isolable product, the stepwise reaction of **1** with $CrCl_2$ and lithium could provide pentalithio spiro chromacycle **3** as dark green crystals in 63% yield.

Characterization. The single crystals of **2** and **3** could be obtained by recrystallization in the mixed solvent of hexane, Et_2O, and THF at −20 °C. Their molecular structures were determined by X-ray single-crystal structural analyses. As shown in Fig. 1c, complex **2** features three vanadacycles spiro-fused by one V atom. The averaged C–V–C angle within the vanadacycles is 74.7°, and the averaged *trans* C–V–C angle is 160.9°, indicating a distorted octahedral geometry with approximate D_3 symmetry. For each vanadacycle there are two Li cations bonded in η^5 mode. All three vanadacycles are nearly planar with almost vanishing folding angles (0.1°, 1.7°, and 0.5°). The C–C bond lengths within the 5-membered rings are remarkably averaged compared to those in **1** (1.4305(19), 1.513(2), 1.4295(18) Å). Meanwhile, the C–C bond length alternation in the phenyl rings increases slightly (Supplementary Fig. 3). These features indicate considerable electron back donation from the V center to the biphenyl ligands and thus hint at a possible metalla-aromatic structure[29,30]. Organovanadium complexes with six V–C σ bonds are very rare[31], complex **2** is a structurally well-defined tris-spiro vanadacycle with six V–C σ bonds.

As shown in Fig. 1c, complex **3** also has a tris-spiro scaffold. Two of the chromacycles (Rings A and B) have two η^5 bonded Li cations, while the other one (Ring C) has only one η^5 bonded Li cation, which is coordinated by two THF molecules. This might be resulted from the relatively weaker interaction between the Li cation and "monoanionic" Ring C, as reflected by the larger Li–ring distance (2.082 Å) compared to those of Ring A (avg. 1.874 Å) and Ring B (avg. 1.848 Å). One of the Li cations bonded to Ring A is coordinated by Et_2O, probably due to the reduced steric hindrance. Rings A and B have nearly planar structures with averaged C–C bonds within the 5-membered rings, which is similar to the vanadacycles in **2** but distinct from the reported "neutral" chromafluorene (1.419 (4), 1.464(4), 1.425(4) Å)[32]. However, Ring C has a larger folding angle (8.4°) and a C–C bond alternation analogous to that reported for non-aromatic dilithionickelafluorene (1.438 (5), 1.479(6), 1.427(5) Å)[17]. These features imply that Rings A and B have a metalla-aromatic structure whereas Ring C does not.

As both **2** and **3** have an odd number of electrons, EPR spectroscopy was employed to probe their electronic structures. The measured EPR spectrum of **2** (Fig. 2a) at the base temperature showed an octet signal centered at $g \sim 2.0$, thereby indicating that **2** possesses an $S = 1/2$ ground state as $[V(bpy)_3]$[33] and $[V(^tbpy)_3]$[34] (bpy = 2,2′-bipyridine, and ^tbpy = 4,4′-di-*tert*-butyl-2,2′-bipyridine), which elicit similar EPR spectra. The eight lines are due to the hyperfine splitting of ^{51}V ($I = 7/2$, 99.75% abundance). Simulations yielded $g_{x,y,z} = 2.006, 2.005, 2.005$, and $A_{x,y,z} = 77.2, 81.8, 33.1 \times 10^{-4}$ cm^{-1}. The observed large magnitude of A suggested that the unpaired electron primarily resides in a V 3d based orbital. In analogy to $[Cr(^tbpy)_3](PF_6)$[35], the EPR spectrum of **3** (Fig. 2b) exhibited a nearly axial feature at $g \sim 2.0$ flanked by a pair of satellite peaks at both sides originating from the hyperfine interaction of ^{53}Cr ($I = 3/2$, 9.50% abundance). Consequently, **3** also features a doublet ground state. Simulations gave $g_{x,y,z} = 2.015, 2.010, 2.001$, and $A_{iso} = 21.3 \times 10^{-4}$ cm^{-1}. The large hyperfine coupling constant of ^{53}Cr demonstrates that the unpaired electron in **3** is predominantly located in the Cr center as found for $[Cr(^tbpy)_3](PF_6)$[35].

To gain more insight into the oxidation states of the metal centers in **2** and **3**, X-ray photoelectron spectroscopy (XPS) experiments were also carried out. The XPS of **2** detected the V $2p_{3/2}$ binding energy (BE) at 517.2 eV (Supplementary Fig. 7). Although no octahedral V complex with similar BE was found in the NIST XPS database, this BE value is notably higher than those of $K_4[V(CN)_6]$ (513.3 eV)[36] and $V(acac)_3$ (514.2 eV)[37] as archetypal octahedral V(II) and V(III) complexes, which suggests that the oxidation state of V in **2** is most likely higher than +3. The Cr $2p_{3/2}$ BE of **3** was observed at 577.5 eV (Supplementary Fig. 8), similar to those of $Cr(SCN)_6(PPh_4)_3$ (577.4 eV)[38] and $Cr(acac)_3$ (577.7 eV)[39], thereby indicating a Cr(III) center in **3**.

DFT calculations. Based on the experimental findings, DFT calculation was carried out to further elucidate the electronic structures of **2** and **3**. The optimized structures of **2** and **3** agree well with their single crystal structures (Supplementary Tables 4 and 5). As shown in Fig. 3a, in the upper valence region of complex **2**, one can identify five singly occupied molecular orbitals (MOs) with considerable V 3d character. Among them, one is an essential nonbonding V d_{z2} based orbital with predominant V parentage (80%). The other four MOs form two spin coupled pairs and represent the bonding combination between the V d_{xy} and d_{x2-y2} orbitals and the group orbital of e symmetry composed of the π* orbitals of the three biphenyl ligands[40]. It should be noted that the V contributions in these four MOs are less than 50%. In other words, the four electrons are delocalized on the V center and the three ligands. This result indicates that the metal-ligand interaction is rather covalent; thus, the physical oxidation state of the V center cannot be unambiguously assigned, and the bonding of **2** is best interpreted as a resonance hybrid of a range of limiting electronic-structure descriptions (Supplementary Fig. 12)[41]. Despite this, on the grounds of the computed V percentage, the one involving a $3d^1$ V(IV) center makes a dominant contribution to the resonance hybrid, consistent with the EPR and XPS measurements. Specifically, the observation that the unpaired electron of **2** predominantly locates in the d_{z2} centered singly occupied MO is consistent with its $A_{x,y,z}$ matrix with two large and one small components. Because the biphenyl π* orbital is bonding in nature with respect to the C_β–C_β bond but antibonding with respect to the C_α–C_β bond, the electron population of this π* orbital should lead to a lengthening of the C_α–C_β bond and shortening of the C_β–C_β bond, which accounts for the observed equalization of the C–C bond lengths of the three vanadacycles in **2**.

As shown in Fig. 3b, complex **3** also has five singly occupied MOs with considerable Cr 3d character, and one of them is the nonbonding Cr d_{z2} based orbital. The other four MOs have negligible contribution from Ring C since the Cr d_{xy} and d_{x2-y2} orbitals preferentially interact with the π* orbitals of Rings A and B, a situation different from **2**. This can be traced back to the more pronounced geometric distortions of **3** from the idealized D_3 symmetry. In these four MOs, the two spin-up ones possess dominant Cr percentages (> 70%), while the two spin-down ones are essentially the biphenyl π* orbitals. The electronic structure of **3** is thus best viewed as having a high-spin Cr(III) center that is antiferromagnetically coupled to two trianionic biphenyl radicals and chelated by another closed-shell dianionic ligand yielding an overall doublet ground state, viz. $Li_5Cr(III)(L^{2-})(L^{\bullet3-})_2$. This bonding description agrees with that deduced from the EPR and XPS measurements, and is reminiscent of our previous reported spiroaromatic manganacycle with two independent 6π aromatic rings[19].
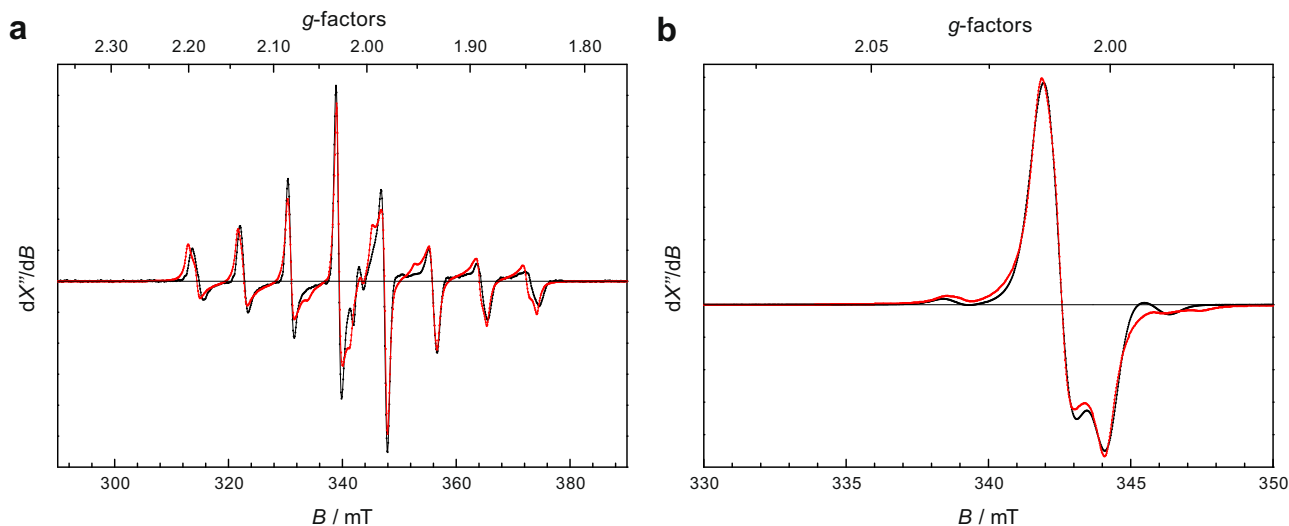
Fig. 2 X-band EPR spectra of complexes 2 and 3 (black trace) and simulation (red trace). a Spectrum of **2** recorded at 30 K. **b** Spectrum of **3** recorded at 40 K.
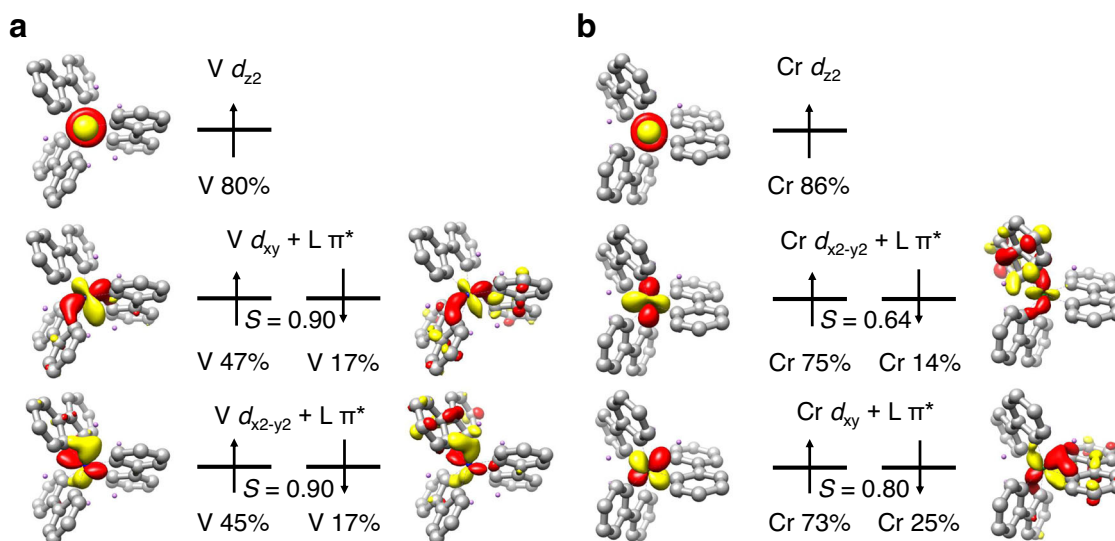

Fig. 3 Schematic MO diagrams. S is the spatial overlap between the two orbitals of a given spin coupled pair. Schematic MO diagrams of complexes **2** (**a**) and **3** (**b**).

According to our previous investigations[17–19], strong d-π^* interactions between the metal center and the ligands as those found for **2** and **3** might induce metalla-aromaticity. To further verify this hypothesis, a series of theoretical methods were employed. The NICS value, a widely used index to evaluate aromaticity[42,43], was calculated for the five-membered metalla-cycles in **2** and **3**. The calculated NICS(1)$_{zz}$ values for the three vanadacycles in **2** were −24.9, −26.0, and −24.4 ppm, indicating three metalla-aromatic rings. For complex **3**, Rings A and B are metalla-aromatic as suggested by the estimated NICS(1)$_{zz}$ values of −18.5 and −19.5 ppm, while Ring C with an almost vanishing NICS(1)$_{zz}$ value of −3.1 ppm is essentially non-aromatic. A similar trend was found for the calculated NICS(0) and NICS(0)$_{zz}$ values (Supplementary Table 6). For comparison, we also conducted a computational study on the aforementioned Ta (DAD)$_3$$^+$, which was proposed to be a tris-spiroaromatic species by Rzepa[25]. However, the NICS(1)$_{zz}$ values turned out to be −1.2 ppm for all its three metallacycles, indicating non-aromaticity. This difference might arise from the lower π-HOMO-LUMO gap of dilithiobiphenyl **1** (4.42 eV) compared with DAD ligand (5.87

eV), which leads to an increasing covalency of the metal-ligand interaction and a higher degree of electron delocalization in complex **2**.

For complex **2**, in addition to the four electrons in the d-π^* bonding orbitals shown in Fig. 3a, each biphenyl ligand also possesses 12 π electrons, thereby leading to a 40π Craig-Möbius aromatic system. Correspondingly, 20 pairs of singly occupied π-type MOs could be identified for **2** (20 spin-up and 20 spin-down, Supplementary Fig. 13), based on which the ELF-π analysis[44,45] was undertaken. As shown in Fig. 4a, there is a substantial electron delocalization in the π orbitals of the three ligands circulated by the V d orbitals. The bifurcation values (BVs) of ELF-π on the three ligands are similar (Supplementary Fig. 14), suggesting an almost equal electron delocalization on them, and the BVs on Ring A is shown in Fig. 4b as an example. For comparison, the ELF-π BVs of dilithiobiphenyl **1** were also calculated and the result revealed that the electron delocalization on two phenyl rings is independent. Compared with **1**, complex **2** has smaller BVs at C$_\alpha$–C$_\beta$ (**1**: 0.87; **2**: 0.61, 0.62) and a larger BV at C$_\beta$–C$_\beta$ (**1**: 0.33; **2**: 0.60), consistent with the single crystal bond

a

b

c

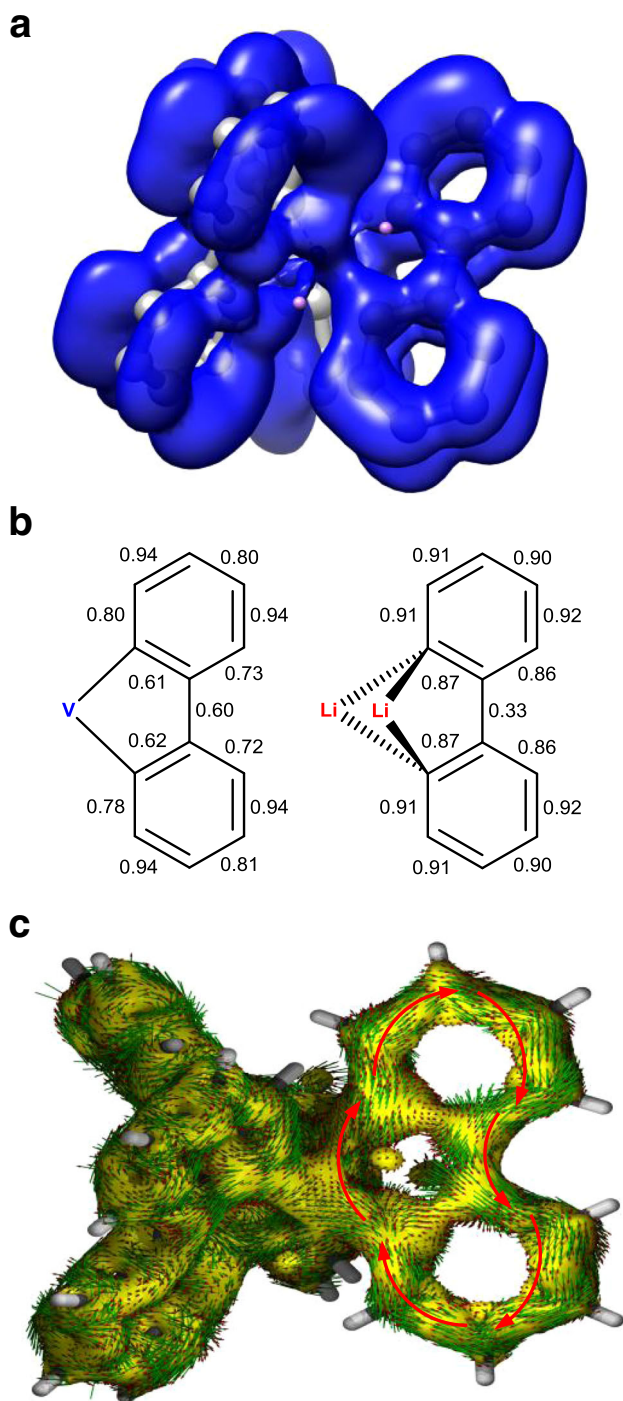**Fig. 4 Analyses on the aromaticity of complex 2. a** The ELF-π isosurface of **2** at 0.35. **b** ELF-π bifurcation values of the biphenyl ligands in **2** (Ring A) and **1**. **c** AICD plot of **2** from π contribution. AICD isosurface of 0.03 is shown in yellow. Red arrows represent the direction of the ring current. The magnetic field vector is orthogonal to the ring plane and points outside (clockwise currents are diatropic).

lengths and the considerable electron density in the π* orbitals. This difference demonstrates that the strong d-π* interaction in **2** results in complete π electron delocalization over the entire complex and thus a metalla-aromatic structure.

AICD plot is a widely applied method for visualizing induced ring current[46,47]. Based on the 20 pairs of π-type MOs, AICD-π analysis was performed. As shown in Fig. 4c, when an external magnetic field is applied perpendicular to the vandacycle (e.g.,

Ring A in **2**), a strong diamagnetic ring current is generated over the V atom and the ligand, indicating a metalla-aromatic system.

As the coordinated Li cations in the dilithiometallole have been found to be indispensable to metalla-aromaticity in our previous work[19], we also examined the hypothetical hexaanion **2′** by removing the six Li cations and THF in **2** without further geometry optimization. As a result, only one d-π* bonding orbital involving Rings A and C was found in **2′** (Supplementary Fig. 16). The calculated NICS(1)$_{zz}$ values indicated that Ring A (−12.7, 4.0 ppm) and Ring C (−13.5, 0.3 ppm) in **2′** have negligible aromatic character while Ring B (−2.5, 1.1 ppm) is essentially non-aromatic (Supplementary Fig. 17). In addition, the geometry optimization starting from **2′** was also conducted, and the resulting species **2″** features remarkable C–C bond alternation in Rings A and B (Supplementary Fig. 18). These results reveal that the Li cations increase the electron affinity of the three dianoinic biphenyl ligands and strengthen the electron back donation from the V center to them. Consequently, the enhanced electron delocalization between the metal center and the ligands leads to 40π Craig-Möbius aromaticity of **2**.

Complexes **2** and **3** have a similar scaffold, but differ by the number of coordinated Li cations, we thus surmise that the latter could be a key factor to dictate their distinct aromaticity. Indeed, when adding one Li cation to Ring C in **3**, the resulting hypothetical cation **4** features three metalla-aromatic rings in analogy to **2**, as indicated by the calculated NICS values (Supplementary Table 6) and the averaged C–C bond lengths (Supplementary Table 7). Although **4** and **2** feature an analogous bonding situation, the four d-π* MOs in **4** possess more Cr d character (72%, 72%, 24%, 24%, Supplementary Fig. 19), suggesting weaker Cr-to-biphenyl ligand back donation in **4**. This largely arises from the higher effective nuclear charge of Cr than that of V. Consequently, the lower energy of the Cr orbitals diminishes the extent of the back donation. This results in a lower degree of the electron delocalization in chromacycles, consistent with their less negative NICS values compared to those found for vanadacycles. In addition, we also examined the hypothetical anion **5** by removing one Li cation from Ring C in **2** and a similar trend was observed between **3** and **5** (Supplementary Table 6, Supplementary Fig. 19). These findings further corroborate the notion that the presence of Li cations is crucial for the extended aromaticity, and underscore the important role played by spiro atoms, which can influence the degree of the electron delocalization.

In summary, hexalithio spiro vanadacycle **2** was synthesized and characterized to be a tris-spiroaromatic complex. The V center uses its two 3d orbitals to interact with π* orbitals of the three biphenyl ligands, forming a 40π Craig-Möbius aromatic system. Pentalithio spiro chromacycle **3** was also prepared, in which preferential interaction of the two Cr 3d orbitals with two biphenyl ligands leads to the formation of two independent metalla-aromatic rings. This work presents a class of spiroaromatic complexes and highlights the pivotal role of transition metals, due to its flexible bonding modes, in realizing aromaticity.

Methods

General information. Unless otherwise noted, all starting materials were commercially available and were used without further purification. Solvents were purified with an Mbraun SPS-800 Solvent Purification System. All reactions were carried out under a dry and oxygen-free nitrogen atmosphere by using Schlenk techniques or under an argon atmosphere in a Vigor (SG1200/750TS-F) glovebox. The argon in the glovebox was constantly circulated through a copper/molecular sieve catalyst unit. The oxygen and moisture concentrations in the glovebox atmosphere were monitored by an O_2/H_2O Combi-Analyzer to ensure both were always below 1 ppm. Elemental analysis was carried out using an Elementar Vario EL Cube elemental analyser. XPS was carried out on an Axis Ultra imaging photoelectron spectrometer. Solution magnetic susceptibility measurements were performed by the Evans method[48] using a Bruker ARX400 spectrometer. IR spectra

were recorded using a Bruker ALPHA II FTIR spectrometer. UV–vis spectra were recorded using an Agilent Cary 60 UV–vis spectrophotometer. X-band cw-EPR measurements were performed on a Bruker E500 ELEXSYS spectrometer equipped with the Bruker dual-mode cavity (ER4116DM) and an Oxford Instruments helium flow cryostat (ESR 900). The microwave bridge was the high-sensitivity bridge Super-X from Bruker (ER-049X) with an integrated microwave frequency counter. The magnetic field controller (ER032T) was externally calibrated with a Bruker NMR field probe (ER035M). The spin Hamiltonian simulations were performed with the program esimX developed by Dr. E. Bill.

Synthesis of complex 1[49]. Under a nitrogen atmosphere, ^{n}BuLi in hexane (7.8 mL, 2.7 mol/L, 21 mmol) was added dropwise to a solution of 2,2′-dibromo-1,1′-biphenyl (3.120 g, 10 mmol) in diethyl ether (50 mL) at −78 °C. The mixture was stirred at −78 °C for 30 min and then warmed to room temperature and stirred for 3 h. The solvent was removed in vacuum and the residue was washed with hexane (15 mL × 3) and dried under vacuum. Complex **1** was obtained as a white solid. Yield: 1.560 g, 94%.

Synthesis of complex 2. In an argon atmosphere glovebox, a suspension of dilithiobiphenyl **1** (0.0747 g, 0.45 mmol) in Et_2O (4 mL) was added into the mixture of $VCl_3(THF)_3$ (0.0560 g, 0.15 mmol) and metallic lithium (0.0345 g, 5.0 mmol) in Et_2O (2 mL). Then THF (2 mL) was added drop by drop and the mixture was stirred at room temperature for 12 h. The solvent was removed under vacuum and the residue was extracted with toluene and filtered. The filtrate was recrystallized in the mixed solvent of hexane/Et_2O/THF (10:10:1) at −20 °C and complex **2** was obtained as dark blue crystals. The crystals were washed with cold hexane and dried under vacuum. Yield: 79.9 mg, 54%. Analysis (calcd., found for $C_{60}H_{72}Li_6O_6V$): C: 73.40, 73.24; H, 7.39, 7.55. Magnetic susceptibility (Evans'-method): $\mu_{eff} = 2.1 \pm 0.1\ \mu_B$ in THF-d_8 at 298 K. IR (KBr, cm^{-1}) υ: 3020 (m), 2975 (m), 2926 (m), 2876 (m), 1547 (w), 1487 (w), 1388 (s), 1269 (s), 1228 (m), 1195 (m), 1140 (m), 1041 (m), 954 (s), 936 (s), 900 (s), 725 (s), 471 (w).

Synthesis of complex 3. In an argon atmosphere glovebox, a suspension of dilithiobiphenyl **1** (0.0747 g, 0.45 mmol) in Et_2O (4 mL) was added into the mixture of $CrCl_2$ (0.0184 g, 0.15 mmol) and Et_2O (2 mL). Then THF (2 mL) was added drop by drop. After stirred at room temperature for 5 h, metallic lithium (0.0345 g, 5.0 mmol) was added. and the mixture was stirred at room temperature for 12 h. The solvent was removed in vacuum and the residue was extracted with toluene and filtered. The filtrate was recrystallized in the mixed solvent of hexane/Et_2O/THF (10:10:1) and complex **3** was obtained as dark green crystals. The crystals were washed with cold hexane and dried under vacuum. Yield: 85.9 mg, 63%. Analysis (calcd., found for $C_{56}H_{66}CrLi_5O_5$): C: 74.25, 73.63; H, 7.34, 7.31. A satisfying result for carbon content of **3** could not be obtained due to its extreme sensitivity to air. Magnetic susceptibility (Evans'method): $\mu_{eff} = 3.0 \pm 0.1\ \mu_B$ in THF-d_8 at 298 K. IR (KBr, cm^{-1}) υ: 3026 (m), 2975 (m), 2925 (s), 2877 (m), 2854 (m), 1550 (m), 1459 (m), 1410 (m), 1390 (s), 1271 (s), 1228 (m), 1203 (m), 1198 (m), 1146 (m), 1042 (s), 957 (s), 909 (m), 891 (m), 738 (s), 729 (s), 466 (w), 454 (w).

Computational details. DFT calculations were carried out using the ORCA quantum chemical program package[50]. Geometry optimizations were performed with the (U)B3LYP[51,52] density functional in combination with D3(BJ) dispersion correction[53,54]. Vanadium, chromium, and tantalum atoms were treated with a Stuttgart effective core potential[55,56] and Pople's basis set 6-311 G(d,p)[57] was used for other elements. ELF-π analysis was performed using the Multiwfn program[58].

Data availability
Crystallographic data for the structures reported in this article have been deposited at the Cambridge Crystallographic Data Centre under deposition numbers CCDC 2033720 (**1**), CCDC 1984387 (**2**), and CCDC 1984388 (**3**) and are available from CCDC in cif format. These data can be obtained free of charge from The Cambridge Crystallographic Data Centre via www.ccdc.cam.ac.uk/data_request/cif. All other data supporting the findings of this study are available within the article and its Supplementary Information, or from the corresponding author upon reasonable request. Cartesian coordinates of the DFT optimized structures are provided in Supplementary Data 1.

References
1. Schleyer, Pv. R. Introduction: aromaticity. *Chem. Rev.* **101**, 1115–1118 (2001).
2. Herges, R. Topology in chemistry: designing Möbius molecules. *Chem. Rev.* **106**, 4820–4842 (2006).
3. Hua, Y., Zhang, H. & Xia, H. Aromaticity: history and development. *Chin. J. Org. Chem.* **38**, 11–28 (2018).
4. Saito, M. et al. Dilithioplumbole: a lead-bearing aromatic cyclopentadienyl analog. *Science* **328**, 339–342 (2010).
5. Velian, A. & Cummins, C. C. Synthesis and characterization of P2N3−: an aromatic ion composed of phosphorus and nitrogen. *Science* **348**, 1001–1004 (2015).
6. Peeks, M. D., Claridge, T. D. W. & Anderson, H. L. Aromatic and antiaromatic ring currents in a molecular nanoring. *Nature* **541**, 200–203 (2017).
7. Pagano, J. K. et al. Actinide 2-metallabiphenylenes that satisfy Hückel's rule. *Nature* **578**, 563–567 (2020).
8. Thorn, D. L. & Hoffmann, R. Delocalization in metallocycles. *Nouv. J. Chim.* **3**, 39–45 (1979).
9. Mauksch, M. & Tsogoeva, S. B. Demonstration of "Möbius" aromaticity in planar metallacycles. *Chem. Eur. J.* **16**, 7843–7851 (2010).
10. Frogley, B. J. & Wright, L. J. Recent advances in metallaaromatic chemistry. *Chem. Eur. J.* **24**, 2025–2038 (2018).
11. Wei, J., Zhang, W.-X. & Xi, Z. The aromatic dianion metalloles. *Chem. Sci.* **9**, 560–568 (2018).
12. Zhu, C. & Xia, H. Carbolong chemistry: a story of carbon chain ligands and transition metals. *Acc. Chem. Res.* **51**, 1691–1700 (2018).
13. Chen, D., Xie, Q. & Zhu, J. Unconventional aromaticity in organometallics: the power of transition metals. *Acc. Chem. Res.* **52**, 1449–1460 (2019).
14. Chen, D., Hua, Y. & Xia, H. Metallaaromatic chemistry: history and development. *Chem. Rev.* **120**, 12994–13086 (2020).
15. Zhu, C. et al. Stabilization of anti-aromatic and strained five-membered rings with a transition metal. *Nat. Chem.* **5**, 698–703 (2013).
16. Zhu, C. et al. Planar Möbius aromatic pentalenes incorporating 16 and 18 valence electron osmiums. *Nat. Commun.* **5**, 3265 (2014).
17. Wei, J., Zhang, W.-X. & Xi, Z. Dianions as formal oxidants: synthesis and characterization of aromatic dilithionickeloles from 1,4-dilithio-1,3-butadienes and [Ni(cod)2]. *Angew. Chem. Int. Ed.* **54**, 5999–6002 (2015).
18. Zhang, Y. et al. Spiro metalla-aromatics of Pd, Pt, and Rh: synthesis and characterization. *J. Am. Chem. Soc.* **139**, 5039–5042 (2017).
19. Zhang, Y. et al. Tetralithio metalla-aromatics with two independent perpendicular dilithio aromatic rings spiro-fused by one manganese atom. *Angew. Chem. Int. Ed.* **58**, 9625–9631 (2019).
20. Simmons, H. E. & Fukunaga, T. Spiroconjugation. *J. Am. Chem. Soc.* **89**, 5208–5215 (1967).
21. Hoffmann, R., Imamura, A. & Zeiss, G. D. Spirarenes. *J. Am. Chem. Soc.* **89**, 5215–5220 (1967).
22. Semmelhack, M. F., De Franco, R. J., Margolin, Z. & Stock, J. Kinetic acidity as a probe for spiroaromaticity in a spiro[2.3]hexadiene. *J. Am. Chem. Soc.* **94**, 2115–2116 (1972).
23. Rzepa, H. S. & Taylor, K. R. Möbius and Hückel spiroaromatic systems. *J. Chem. Soc. Perkin Trans.* **2**, 1499–1501 (2002).
24. Hall, D. & Rzepa, H. S. Möbius bis and tris-spiroaromatic systems. *Org. Biomol. Chem.* **1**, 182–185 (2003).
25. Rzepa, H. S. Möbius aromaticity and delocalization. *Chem. Rev.* **105**, 3697–3715 (2005).
26. Daff, P. J., Etienne, M., Donnadieu, B., Knottenbelt, S. Z. & McGrady, J. E. Stable formally zerovalent and diamagnetic monovalent niobium and tantalum complexes based on diazadiene ligands. *J. Am. Chem. Soc.* **124**, 3818–3819 (2002).
27. Neugebauer, W., Kos, A. J. & Schleyer, P. V. R. Regioselektive dimetallierung von aromaten. Bequemer zugang zu 2,2′-disubstituierten biphenylderivaten. *J. Organomet. Chem.* **228**, 107–118 (1982).
28. Schubert, U., Neugebauer, W. & Schleyer, P. V. R. Symmetrical double lithium bridging in 2,2′-di(lithium-tmeda)biphenyl (tmeda = MeNCH₂CH₂NMe₂): experimental confirmation of theoretical predictions. *J. Chem. Soc., Chem. Commun.* 1184–1185 (1982).
29. Liu, Y. et al. Chemistry of the aromatic 9-germafluorenyl dianion and some related silicon and carbon species. *J. Am. Chem. Soc.* **124**, 12174–12181 (2002).
30. Saito, M., Shimosawa, M., Yoshioka, M., Ishimura, K. & Nagase, S. Synthesis and characterization of dimetallostannafluorenes. *Chem. Lett.* **35**, 940–941 (2006).
31. Olmstead, M. M., Power, P. P. & Shoner, S. C. Isolation and X-ray crystal structures of the homoleptic, σ-bonded, transition-metal aryl complexes [(LiEt₂O)₄VPh₆] and [(LiEt₂O)₃CrPh₆]. *Organometallics* **7**, 1380–1385 (1988).
32. Agapie, T., Schofer, S. J., Labinger, J. A. & Bercaw, J. E. Mechanistic studies of the ethylene trimerization reaction with chromium−diphosphine catalysts: experimental evidence for a mechanism involving metallacyclic intermediates. *J. Am. Chem. Soc.* **126**, 1304–1305 (2004).
33. Rieger, A. L., Scott, J. L. & Rieger, P. H. Electron spin resonance of tris(2,2′-bipyridyl)vanadium(0). *Inorg. Chem.* **33**, 621–622 (1994).

34. Bowman, A. C., Sproules, S. & Wieghardt, K. Electronic structures of the [V(^{t}bpy)$_3$]^z (z = 3+, 2+, 0, 1−) electron transfer series. *Inorg. Chem.* **51**, 3707–3717 (2012).

35. Scarborough, C. C., Sproules, S., Weyhermüller, T., DeBeer, S. & Wieghardt, K. Electronic and molecular structures of the members of the electron transfer series [Cr(^{t}bpy)$_3$]^n (n = 3+, 2+, 1+, 0): an X-ray absorption spectroscopic and density functional theoretical study. *Inorg. Chem.* **50**, 12446–12462 (2011).

36. Vannerberg, N. G. The ESCA-spectra of sodium and potassium cyanide and of the sodium and potassium salts of the hexacyanometallates of the first transition metal series. *Chem. Scr.* **9**, 122–126 (1976).

37. Larsson, R., Folkesson, B. & Schon, G. X-ray photoelectron spectroscopy and homogenous catalysis. I. Vanadium compounds. *Chem. Scr.* **3**, 88–90 (1973).

38. Folkesson, B. & Larsson, R. An ESCA investigation of some thiocyanato complexes. *J. Electron Spectrosc. Relat. Phenom.* **26**, 157–166 (1982).

39. Allen, G. C. & Tucker, P. M. Multiplet splitting of X-ray photoelectron lines of chromium complexes. The effect of covalency on the 2p core level spin-orbit separation. *Inorg. Chim. Acta* **16**, 41–45 (1976).

40. Wang, M., Weyhermüller, T., Bill, E., Ye, S. & Wieghardt, K. Structural and spectroscopic characterization of rhenium complexes containing neutral, monoanionic, and dianionic ligands of 2,2′-bipyridines and 2,2′:6,2′′-terpyridines: an experimental and density functional theory (DFT)-computational study. *Inorg. Chem.* **55**, 5019–5036 (2016).

41. Ye, S., Geng, C. –Y., Shaik, S. & Neese, F. Electronic structure analysis of multistate reactivity in transition metal catalyzed reactions: the case of C–H bond activation by non-heme iron(IV)–oxo cores. *Phys. Chem. Chem. Phys.* **15**, 8017–8030 (2013).

42. Schleyer, Pv. R., Maerker, C., Dransfeld, A., Jiao, H. & Hommes, N. J. Rv. E. Nucleus-independent chemical shifts: a simple and efficient aromaticity probe. *J. Am. Chem. Soc.* **118**, 6317–6318 (1996).

43. Fallah-Bagher-Shaidaei, H., Wannere, C. S., Corminboeuf, C., Puchta, R. & Schleyer, P. V. R. Which NICS aromaticity index for planar π rings is best? *Org. Lett.* **8**, 863–866 (2006).

44. Becke, A. D. & Edgecombe, K. E. A simple measure of electron localization in atomic and molecular systems. *J. Chem. Phys.* **92**, 5397–5403 (1990).

45. Silvi, B. & Savin, A. Classification of chemical bonds based on topological analysis of electron localization functions. *Nature* **371**, 683–686 (1994).

46. Herges, R. & Geuenich, D. Delocalization of electrons in molecules. *J. Phys. Chem. A* **105**, 3214–3220 (2001).

47. Geuenich, D., Hess, K., Köhler, F. & Herges, R. Anisotropy of the induced current density (ACID), a general method to quantify and visualize electronic delocalization. *Chem. Rev.* **105**, 3758–3772 (2005).

48. Evans, D. F. The determination of the paramagnetic susceptibility of substances in solution by nuclear magnetic resonance. *J. Chem. Soc.* 2003–2005 (1959).

49. Shao, C., Zhou, B., Wu, Z., Ji, X. & Zhang, Y. Synthesis of carbazoles from 2-iodobiphenyls by palladium-catalyzed C-H activation and amination with diaziridinone. *Adv. Synth. Catal.* **360**, 887–892 (2018).

50. Neese, F. The ORCA program system. *WIREs Comput. Mol. Sci.* **2**, 73–78 (2012).

51. Becke, A. D. Density-functional thermochemistry. III. The role of exact exchange. *J. Chem. Phys.* **98**, 5648–5652 (1993).

52. Lee, C. T., Yang, W. T. & Parr, R. G. Development of the Colle-Salvetti correlation-energy formula into a functional of the electron density. *Phys. Rev. B* **37**, 785–789 (1988).

53. Grimme, S., Antony, J., Ehrlich, S. & Krieg, H. A consistent and accurate ab initio parameterization of density functional dispersion correction (DFT-D) for the 94 elements H-Pu. *J. Chem. Phys.* **132**, 154104 (2010).

54. Grimme, S., Ehrlich, S. & Goerigk, L. Effect of the damping function in dispersion corrected density functional theory. *J. Comp. Chem.* **32**, 1456–1465 (2011).

55. Dolg, M., Wedig, U., Stoll, H. & Preuss, H. Energy-adjusted ab initio pseudopotentials for the first row transition elements. *J. Chem. Phys.* **86**, 866–872 (1987).

56. Andrae, D., Haeussermann, U., Dolg, M., Stoll, H. & Preuss, H. Energy-adjusted ab initio pseudopotentials for the 2nd and 3rd row transition-elements. *Theor. Chem. Acc.* **77**, 123–141 (1990).

57. Krishnan, R., Binkley, J. S., Seeger, R. & Pople, J. A. Self-consistent molecular orbital methods. XX. A basis set for correlated wave functions. *J. Chem. Phys.* **72**, 650–654 (1980).

58. Lu, T. & Chen, F.-W. Multiwfn: a multifunctional wavefunction analyzer. *J. Comput. Chem.* **33**, 580–592 (2012).

Author contributions

Z.H. carried out the synthesis, X-ray and XPS characterizations, DFT calculations, and wrote the manuscript. Y.Z. assisted the synthesis and characterizations. S.Y. conducted EPR experiments and simulations. W.-X.Z., S.Y., J.W., and Z.X. designed the project, analyzed the data, and revised the manuscript.

Competing interests

The authors declare no competing interests.

Additional information

Supplementary information The online version contains supplementary material available at https://doi.org/10.1038/s41467-021-21648-9.

Correspondence and requests for materials should be addressed to J.W., S.Y. or Z.X.

Reprints and permission information is available at http://www.nature.com/reprints

Publisher's note Springer Nature remains neutral with regard to jurisdictional claims in published maps and institutional affiliations.